Could machine learning break the convection deadlock?

P. Gentine[1], M. Pritchard[2], S. Rasp[3], G. Reinaudi[1] and G. Yacalis[2]

[1]Columbia University, New York, NY 10027.

[2]University of California - Irvine, Irvine, CA 92697.

[3]LMU Munich, Munich, Germany

Corresponding author: Pierre Gentine (pg2328@columbia.edu)

Key Points:

- We use a global atmospheric model with embedded cloud resolving model (super-parameterization) on an aquaplanet, as a training dataset for a machine learning algorithm of convection
- The machine learning algorithm can reproduce most of the key features of the embedded cloud resolving model heating and moistening tendencies
- The machine learning algorithm is reproduce and is more computationally efficient than a super parameterization, but does not behave stochastically

Abstract

Modeling and representing moist convection in coarse-scale climate models remains one of the main bottlenecks of current climate simulations. Many of the biases present with parameterized convection are strongly reduced when convection is explicitly resolved (in cloud resolving models at high spatial resolution ~ a kilometer or so). We here present a novel approach to convective parameterization based on machine learning over an aquaplanet with prescribed sea surface temperatures. The machine learning is trained over a superparameterized version of a climate model in which convection is resolved by an embedded 2D cloud resolving models. The machine learning representation of convection, called Cloud Brain (CBRAIN) replicates many of the convective features of the superparameterized climate model, yet reduces its inherent stochasticity. The approach presented here opens up a new possibility and a first step towards better representing convection in climate models and reducing uncertainties in climate predictions.

Plain Language Summary

The representation of the atmospheric heating and moistening due to moist convection remains a major challenge in current generation of climate models, leading to a large spread in climate prediction. Here we show that machine learning techniques trained on a high resolution model in which moist convection is resolved can be an appealing technique to tackle and better represent moist convection in coarse resolution calimte models.

1 Introduction

Convective parameterization remains one of the main roadblocks to weather and climate prediction [*Stevens and Bony*, 2013; *Medeiros et al.*, 2014; *Sherwood et al.*, 2014; *Bony et al.*, 2015]. Most convective schemes exhibit biases in the vertical structure of heating and moistening, precipitation intensity, and cloud cover [*Daleu et al.*, 2015; 2016]. These errors, in turn, feed back into the larger-scale circulation so that they further inhibit the quality of general circulation model (GCM) simulations and prediction skill [*Bony et al.*, 2015]. One of the main challenges in current convective schemes is also to represent the transitions between different types of convection, such as the transition from shallow to deep convection [*Khouider et al.*, 2003; *Guichard et al.*, 2004; *Khouider and Majda*, 2006; *Wu et al.*, 2009; *Khouider et al.*, 2010; *Dorrestijn et al.*, 2014; *D'Andrea et al.*, 2014; *Rochetin et al.*, 2014a; 2014b; *Couvreux et al.*, 2015], which is especially crucial to predict both continental precipitation and modes of climate variability [Arnold et al., 2014]. In addition, most convective parameterizations do not represent processes, such as convective aggregation, that are essential to accurately predict the response of clouds and precipitation to global warming, outgoing longwave radiation as well as modes of climate variability [*Jeevanjee and Romps*, 2013; *Wing and Emanuel*, 2014; *Arnold and Randall*, 2015; *Bony et al.*, 2015; *Bretherton and Khairoutdinov*, 2015; *Coppin and Bony*, 2015; *Muller and Bony*, 2015].

A typical challenge in convective parameterization is the specification of the plume lateral entrainment [*Cohen*, 2000; *De Rooy et al.*, 2013; *Sherwood and Hernández-Deckers*, 2013; *Yeo and Romps*, 2013; *Tian and Kuang*, 2016], its dependence on environmental conditions (e.g., free tropospheric dryness) [*Derbyshire et al.*, 2004] and the role of subcloud layer organization (due to cold pools or mesoscale heterogeneity) [*Mapes and Neale*, 2011; *D'Andrea et al.*, 2014]. Entrainment is one of the major factors controlling climate sensitivity and explains, to a large extent, the intermodel spread in climate sensitivity in the tropics [*Popke et al.*, 2013]. Entrainment also regulates some of the main features of tropical climate [*Singh and O'Gorman*, 2013] such as the Inter Tropical Convergence Zone (ITCZ) [*Oueslati and Bellon*, 2015], or modes of climate variability [*Bush et al.*, 2015] such as the El Niño or the Madden Julian Oscillation (MJO) [*Kim et al.*, 2012; *Feng et al.*, 2015]. In addition, the representation of the transition between shallow and deep convection is tightly related to changes in updraft entrainment [*Del Genio and Wu*, 2010; *D'Andrea et al.*, 2014], in part due to the organization of the subcloud layer by cold pools [*Khairoutdinov and Randall*, 2006; *D'Andrea et al.*, 2014]. The representation and understanding of entrainment has defied a unified theory even though important progresses have been made in recent years [*Khouider et al.*, 2003; *Khouider and Majda*, 2006; *Khouider et al.*, 2010; *Romps*, 2010; *Mapes and Neale*, 2011; *Dawe and Austin*, 2013; *De Rooy et al.*, 2013; *Sherwood and Hernández-Deckers*, 2013; *Yeo and Romps*, 2013; *Dorrestijn et al.*, 2014; *Feng et al.*, 2015; *Lu et al.*, 2016]. The difficulty behind the presentation of entrainment is that it is inherently a turbulent process, which exhibits random fluctuations. Additional the vertical localization of the initiation of the plume as well as its properties remain a challenge. Detrainment, even if less studied, is also crucial, as its vertical profile determines the structure of the cloud layer and therefore convective instability [*Cohen*, 2000; *De Rooy et al.*, 2013]. In addition, the degree of convective aggregation modifies some of the basic underlying assumptions behind the plume representation (e.g., lack of interaction between plumes) [*Gentine et al.*, 2016].

Current generation of climate models (and typical weather forecast models) with parameterized convection do not capture much of the degree of organization, nor do they represent mesoscale convective systems (MCS), [*Hohenegger and Stevens*, 2016] though the latter are likely essential to accurate simulation and prediction of extreme rainfall events [*Houze*, 2004; *Tan et al.*, 2015]. Finally, another challenge is that climate sensitivity is strongly related to the interaction between deep and shallow convection [*Bony et al.*, 2015], and the coupling between clouds, convection and the large-scale circulation, which is currently poorly captured by parameterized convection [*Bony* *et al.*, 2015; *Daleu et al.*, 2015; *Hohenegger and Stevens*, 2016; *Nie and Sobel*, 2016; *Nie et al.*, 2016].

Many of the previously mentioned problems related to the representation of convection are alleviated when using convective-permitting resolutions, i.e. at horizontal grid spacing of ~2km or less. Convection-permitting models thus offer a promising avenue to address several of those questions. For instance, the transition between shallow and deep convection can be correctly captured at convective permitting scale [*Khairoutdinov and Randall*, 2006; *Khairoutdinov et al.*, 2009]. Convective aggregation is observed at convective permitting scale [*Hohenegger and Stevens*, 2016] and Cloud Resolving Models (CRMs) have been the tool of choice to understand convective aggregation [*Jeevanjee and Romps*, 2013; *Wing and Emanuel*, 2014; *Arnold and Randall*, 2015; *Bony et al.*, 2015; *Bretherton and Khairoutdinov*, 2015; *Coppin and Bony*, 2015; *Muller and Bony*, 2015]. CRMs (at convective permitting scales <2km) also correctly reproduce MSCs and squall lines [*Moncrieff and Liu*, 2006; *Taylor et al.*, 2009], in various conditions, as well as extreme precipitation events driven by larger scale anomalies. CRMs at convective permitting scale can successfully represent the diurnal cycle of precipitation over land and the development of convection from shallow to deep convection [*Guichard et al.*, 2004]. Convective-permitting simulations better represent modes of tropical climate variability [*Arnold et al.*, 2014], and breeze and mesoscale propagation [*Hohenegger et al.*, 2015]. CRMs also correctly capture the feedback between the land surface (and surface heterogeneity) and deep convective triggering [*Hohenegger et al.*, 2009], as well as MCSs triggering, [*Taylor et al.*, 2013].

Therefore, models at convective-permitting scales really appear as “game changers” for the representation of convection. It is however unfeasible at present to use convective resolving scale resolution at the global scale for climate prediction given its computational requirements. To alleviate this problem, one of the most interesting approaches has been to use the so-called "super parameterization (SP)" approach, which computes the vertical heating and moistening profile within a GCM grid by sampling a curtain of an embedded CRM at convective permitting scale [*Khairoutdinov et al.*, 2005; *Goswami et al.*, 2013; *Bretherton and Khairoutdinov*, 2015]. This has led to many successes such as the possibility to rectify the diurnal continental cycle, to improve the representation of the MJO, and to represent both some MCS propagation and some degree of aggregation, and reduce overly strong land-atmosphere coupling [*Pritchard and Somerville*, 2009; *Kooperman et al.*, 2013; 2014; *Pritchard et al.*, 2014; *Benedict and Pritchard*, 2015; *Yu and Pritchard*, 2015; *Kooperman et al.*, 2016a; 2016b; *Sun and Pritchard*, 2016].

In light of this ongoing deadlock, we propose to use an alternative approach to convective parameterization in which convection is represented using a machine-learning algorithm based on Artificial Neural Networks (ANNs),

, trained on cloud-resolving simulations. Clearly, parameterizing convection appears as an ideal problem for the use of machine learning algorithms and especially ANNs. Indeed, machine-learning algorithms have been used in many applications where a clear physically-based algorithm could not be defined. Applications have included self-driving cars, board games (chess and go) [*Silver et al.*, 2016], speech recognition [*Hinton et al.*, 2012], object recognition and detection, medical detection of cancers [*Khan et al.*, 2001; *Zhou et al.*, 2002; *Karabatak and Ince*, 2009], and genomics. There are also applications of ANNs to the geosciences, such as for rainfall prediction (Precipitation Estimation from Remotely Sensed Information using Artificial Neural Networks - PERSIANN - algorithm) [*Moazami et al.*, 2013; *Miao et al.*, 2015; *Tao et al.*, 2016], soil moisture retrieval [*Kolassa et al.*, 2013; 2016; 2017a; 2017b], and retrievals of surface turbulent fluxes [*Jimenez et al.*, 2009; *Alemohammad et al.*, 2016]. In recent years, the development of deep learning and Deep Neural Networks (DNN), i.e., those with multiple hidden layers, has led to important developments in many different fields such as object detection or game strategy learning [*Dahl et al.*, 2011; *Hinton et al.*, 2012; *LeCun et al.*, 2015; *Silver et al.*, 2016; *Tao et al.*, 2016]. One of the advantages of ANNs is that, once trained, they are computationally efficient, as most of the computational burden is dedicated to the training phase.

The goal of this paper is to explore whether short simulations extracted from convective-resolving simulations, which better represent the true physics of convection, can be mined for their essence to build a new class of machine learning-based parameterization. The retrieval is called Cloud Brain (CBRAIN).

2 Data

SuperParameterized Community Atmosphere Model

To evaluate this idea, we use a well validated version of the SuperParameterized Community Atmosphere Model (SPCAM3) in a simplified aquaplanet configuration with zonally symmetric SSTs following a realistic meridional distribution [*Andersen and Kuang* 2012]. Following a 3-month spinup period, we save global data at the host global model timestep frequency (every 30 minutes) representing the arterial inputs to (and outputs from) each of the 8,192 cloud-resolving arrays embedded SPCAM. The simulations are run for 2.5 years, i.e. an equivalent of 450M time instances for training and validation. The first two years are used for training and the validation is performed over the last 0.5 year of the simulation. 30 vertical levels are used in the vertical and the model has a one-degree resolution in both meridional and zonal directions. For the convective tendencies we limited ourselves to the first 21 out of the 30 vertical levels as there was no physics tendencies (beside radiation) at the highest levels. This thus avoids that the retrieval be polluted by noise at higher levels.

3 Methodology

Neural Networks

In this work, we used neural networks (NN) to retrieve the physics tendency. Instead of evaluating only the convective tendencies simulated by SPCAM we decided to estimate directly the entire physics tendency, excluding radiation. The rational for using the full tendency is based on the fact that in practice the microphysics, boundary layer and convective tendencies can be hard to perfectly isolate. In addition, the embedded CRM deviates from an actual CRM in a few subtle ways for seamless integration within the GCM, which strongly limit the isolation of the convective-only tendencies. We thus take the approach to try and reproduce the entire physics tendencies, without radiation. We note that future versions could actually include radiation as a reproducible machine learning algorithm, as is done for instance at the Eruopean Centre For Medium Weather Forecast (ECMWF) [*Chevallier et al.*, 2000].

For the training we use TensorFlow, a recent open-source machine learning framework, from Google along with Keras, a high-level NN API, written in Python and interfacing with TensorFlow. All codes are available on GitHub at https://github.com/gentine/CBRAIN. The training was performed on Graphical Processing Units (NVIDIA K80 and P100) for improved performance, with a performance of roughly 80 batches of size 256 (see below) per second.

The SPCAM dataset is split into a training and validation dataset. To avoid any potential data leakage (i.e. data output inadvertently passed on to the data input), we split the data temporally first, selecting the two first years of the data for training and the remaining 0.5 year for validation. We did not find any dependence on the percentage used for training, as long as at least a full year was used, as the SPCAM outputs are largely sufficient (see discussion below). Several activation functions after the hidden layers (

) were tested and we decided to use a Leaky Rectified Linear Unit, i.e. a Rectified Linear Unit for positive input values: y=x for x>0, but with a slight slope for negative values y=0.03x so that the gradients are always non-null, thus avoiding any potential trapping in non-convergent states. The last activation function is a typically-used linear function.

During the training, the training dataset is divided into small batches of size 256 randomized across latitudes, longitudes and times. Small batches have been shown to be very useful for convergence as they provide a degree of stochasticity to the minimization similarly to stochastic gradient descent. Changing the batch size did not change the results much, however going to 1024 for the batch size reduced the performance, hence why we decided to use a batch of size 256.

We then evaluated the impact of the learning rate and the impact of the time used to divide the learning rate. A learning rate of $2.5\ 10^{-4}$ showed the best performance (with a 20% improvement in R^2) compared to a fast learning rate of 0.025. We then evaluated the impact of time steps needed to half the learning rate and varied it between 5 to 500,000 time steps. The best performance was obtained for 200,000 time steps, with an improvement in terms of R^2 of the order of 20%.

We used two main types of NNs. The first ones are simple feedforward NNs, with different numbers of hidden layers and number of neurons. A second strategy is to use 1D convolutional NNs (CNNs) (basically a filter in the vertical to reduce vertical dimensionality). CNNs have showed dramatic improvements compared to feedforward NNs in many fields of applications such as language translation or image processing [*Krizhevsky et al.*, 2017]. We thus varied the number of hidden layers (depth) and well as the number of neurons (width) to the NNs. We selected the NN with the best performance yet with the minimum number of parameters. Indeed, reducing the number of parameters avoids overfitting and also improved computational efficiency for implementation in full GCM. All input data were first normalized, at each vertical level. A summary of the different model performances, R^2 and RMSE, is presented in Table S1 and S2. Diagnostics were also evaluated at every level to assess which regions of the profiles were the most predictable.

We tested the dependency of the results to different inputs and finally chose the following inputs: temperature and water vapor mixing ration vertical profiles, surface sensible and latent heat fluxes, surface pressure and the adiabatic heating and moistening tendencies from the dynamical core within a time step.

4 Results

We first evaluated the impact of the structure of the different NNs on the retrieval. A summary of different statistics comparing the NN prediction and the SPCAM simulations is presented in Table S1. We note that there are several ways the R^2 statistics can be computed but here we chose to use and sum the variance across all levels, time samples and the variables (here with two variables: the heating and moistening tendencies, where the moistening tendencies are multiplied by Lv/Cp to match the units of the heating tendencies). Similarly, to geometric means, this type of averaging will emphasize errors and thus low overall R^2 will be typical, as higher levels where there is no convection (and thus where an R^2 per level would be close to zero) will lead to small local R^2.

Overall in terms of averaged statistics across levels, neither wide and shallow network (i.e. many neurons but few hidden layers) nor very deeper but narrow networks (i.e. with many layers and few neurons per layer) tended to perform well (Table S1). The best performances were found for relatively wide networks (at least 256 neurons per layers) but with few layers (2 typically). This is different to what is typically found in image processing, in which deeper layers are able to retrieve specific image structures. Even though it is theoretically possible to represent any possible function with a single hidden layer neural network, determining the number of nodes needed in that hidden layer is difficult. Therefore, adding more layers (apart from increasing computational complexity to the training and testing phases), allows for more straightfroward representation of the interactions within the input data, as well as allows for more abstract features to be learned and used as input into the next hidden layer. Deeper networks highlight higher level of abstraction and non-linear combinations between the inputs. The fact that a shallower network (yet with similar degrees of freedom), works better emphasizes that the inputs at different levels and across different variables have more independent impact on the outputs. This is indeed confirmed when using CNNs (Table S2). Little gain is added by the CNNs in terms of performance, compared to the feedforward NNs. This further emphasizes that the inputs of the physics, and in particular convective scheme might be adding information at each level and across each variable used.

A feedforward NN with 1024 neurons in each of the 2 hidden layers was thus selected based on this tradeoff between performance and reduction of the number of parameters (Table S1). It takes roughly a year of samples for the NN retrieval to converge (Figure S1), considering that in our training simulations there are 128 (longitudes) times 64 (latitudes) times 48 (half-hourly) this is equal to 393,216 daily samples. Only marginal changes in convergence are observed with more data sample (given that two full years of data are used for the training), so that less than half of our training dataset is really required.

Investigating the structure of the training, across multiple levels, highlights important differences between the boundary layer, shallow clouds, deep convection and the top of the CRM domain (~1210Pa) (Figure S3). The retrievals systematically yield higher R^2 in the core of the deep convective region (i.e. between 700 and 200hPa), with values above 0.5 and close to 0.8 between 600 and 300hPa. At lower levels, in the shallow convection layer and especially in the boundary layer, the retrieval is degraded with R^2 ranging from 0.25 to 0.4. At very high levels R^2 is negative because there is no convection and there is no predictive power of the NN. This in turn degrades the global metrics across levels (see above, Table S1). It is important to note that SPCAM inherently includes some degree of stochasticity {Subramanian:2017fr}. This is done mainly through the fact that the internal CRM states are restarted randomly at each subtime steps and therefore do not have memory of the large-scale environment except than through the boundary condition forcing. Since feedforward NNs are inherently deterministic they do not reproduce the stochasticity of SP-CAM. This explains that we are unable to perfectly fit the tendencies even with complex NN architectures. Since most of the departure is observed at the lower levels this emphasizes that most of the stochasticity of the physics, mainly through convection, is present in the boundary layer and in the shallow cumulus field. The non-perfect fit also reflects the presence of convective aggregation in the CRMs [*Pauluis and Schumacher*, 2011; *Jeevanjee and Romps*, 2013; *Tobin et al.*, 2013; *Bretherton and Khairoutdinov*, 2015; *Muller and Bony*, 2015; *Holloway*, 2017; *Wing et al.*, 2017], even though the fact that R^2 is much higher in the core of deep convectio (700 to 250hPA), highlights the capacity of the NN to represent some degree of aggregation. It is interesting that there is so much internal variability at lower levels, given that in SPCAM surface fluxes are prescribed homogenously over the GCM grid size and thus are the same across the CRM columns. In the absence of downdrafts and important mesoscale affects the CRM turbulent heat flux profiles should be relatively uniform horizontally. Departure from this homogeneity thus highlights the importance of mesoscale circulations and their natural stochasticity in SPCAM, which cannot be captured by a deterministic NN approach. In addition, decomposing the total vertically integrated R^2 between variables shows that heating tendencies are much better reprdiced by the NN (R2=), compared to moisture (R2=), likely because of wave homogenization for the temperature filed will smoothen the temperature field.

Comparing the vertical and zonal predictions of CBRAIN to SPCAM (Figure 2) shows that CBRAIN correctly reproduces the positions and magnitude of the zonal and meridional average vertical heating and moistening tendencies of SPCAM. In particular, the precipitation structures are nicely captured by CBRAIN. The field is however smoother than the SPCAM field, especially for the moistening tendencies, which tends to be patchier and localized horizontally in SPCAM because of the absence of wave smoothing like in the temperature field. As a result, the difference between CBRAIN and SPCAM heating tendencies are relatively small even though differences appear in regions of strong localized heating. The difference between the CBRAIN and SPCAM moistening tendencies is larger, especially in the tropics. The errors are larger not only near the cores of precipitation but also in shallow convective regions, where the moistening tendencies is large and where SPCAM also exhibits substantial stochasticity, as most of this stochasticity seems to be present at lower levels, in the boundary layer and in the shallow convection field (see previous section). This stochasticity in the boundary layer and shallow convection moistening tendencies in SPCAM is likely due to the reset of the CRM columns at each time step and seem relatively more modest in global CRMs compared to SPCAM [*Satoh et al.*, 2008; *Noda et al.*, 2010][*Seiki et al.*, 2015].

Similar behavior is observed when investigating the vertical and meridional structures of the heating and moistening tendencies. Deep convective events are relatively well reproduced by CBRAIN. However, substantial noise is present in the tropics in the moistening tendencies. The noise between SPCAM and CBRAIN appears relatively random and varies between strong positive and negative anomalies, especially in the strong heating and cooling regions. Again, SPCAM does not exhibit systematic moistening in the shallow cloud region but rather oscillate between strongly positive and strongly negative regions. Such noise is much smaller in the heating tendencies (similar to the meridional and zonal results) and tend to be localized to the lowers levels below deep convection.

4 Discussion and conclusion

We have demonstrated that machine learning, and neural networks in particular, here called CBRAIN, could represent many of features of convective physics for implementation in coarse-grain GCMs. CBRAIN has the advantage to be computationally efficient compared to GCRMs or super-parameterizations. There are, however, important steps required for full implementation of CBRAIN in a GCM. The first and maybe most important limitation of neural networks is that they do not preserve energy and moisture. This can be fine for implementation in a weather forecast model but energy and moisture conversations are absolutely required for climate prediction. Second, typically neural networks are inherently deterministic. It was here shown that the resulting CBRAIN representation of heating and moistening tendencies was too smooth compared to the original SPCAM field used for training, which is more stochastic especially in the lower levels of the atmosphere (below 700hPA). Third, SP used for the training is not without its own unsatisfying trade-offs. The typical use of 2D CRMs corrupts the physics of convective momentum transport [*Khairoutdinov et al.,* 2005; Tulich 2015; *Woelfle et al.* 2018], which impacts the representation of mesoscale convective systems [*Cheng and Xu*, 2014]; the use of limited domain extent artificially throttles vertical mixing by deep convection, corrupting extremes [*Pritchard et al. 2014]*; the use of coarse vertical and horizontal resolution distorts the physics of low clouds [*Parishani et al. 2017*], and the use of periodic boundary conditions limit the propagation of mesoscale convective system, even though some of their features can be captured though convective-wave coupling [*Pritchard et al.*, 2011]. While these issues could conceivably be overcome by enhancing SP to use large, high-resolution 3D CRM domains, this faces the same computational challenges that limit the utility of global CRMs today. Another issue is related to the radiation scheme. In SPCAM or global CRMs the CRM columns are used to compute the radiative tendencies and thus "see" the diversity in cloud cover and potential cloud aggregation. This is not the case in CBRAIN, which still works like a GCM in the sense that a single tendency and a single cloud cover can be computed for the GGCM pixel total domain. A final challenge is related to the fact that inherently the machine learning algorithms is trained on existing data. For climate prediction, the algorithm should be able to generalize correctly to situations that have not have potentially not been seen such as changes in trace gas profiles, concentrations of trace gases or aerosols.

Beside those challenges, we believe that machine learning represents a powerful alternative to typical or embedded-CRM parameterizations. It is computationally efficient, even for relatively large networks. For instance without specific optimization a preliminary test showed that CBRAIN was 10 times faster than SPCAM. CBRAIN is also naturally fitted for data assimilation since computation of the adjoint is straightforward and analytical, making it a natural candidate for operational weather forecasting. Finally, CBRAIN could represent the alternative to current parameterizations, which are still exhibiting too many biases for correct prediction of the future hydrological cycle. As global temperature sensitivity to CO_2 is strongly linked to convective entrainment, this might also improve our estimates of future temperature.

Acknowledgments, Samples, and Data

The codes are available on GitHub at https://github.com/gentine/CBRAIN. The aquaplanet data used here can be requested on demand to Prof. Mike Pritchard, as it is very large (several terabytes) and is hosted on a server at UC-Irvine.

Figures

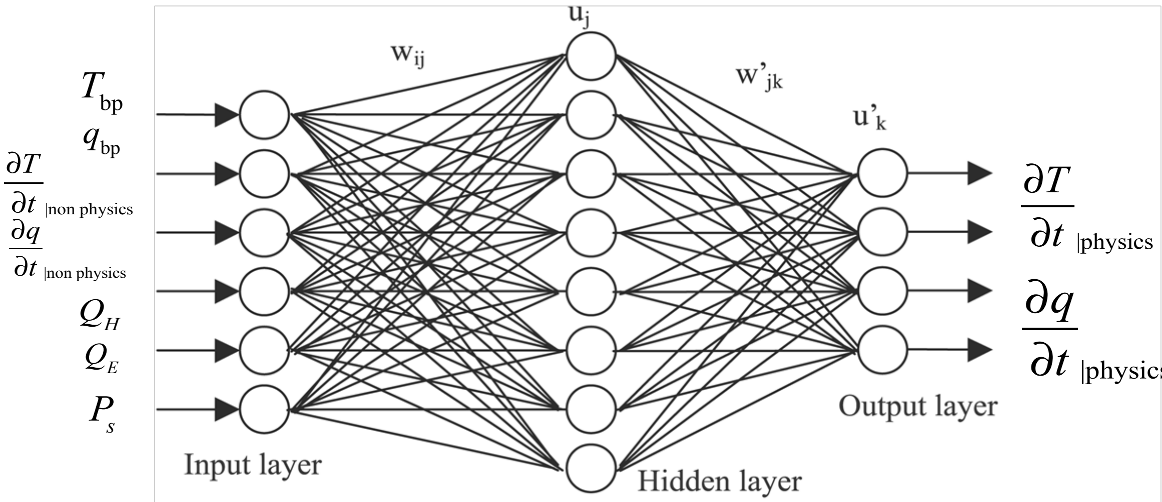

Figure 1: Presentation of a feedforward neural network architecture with one hidden layer and the inputs used as well as the predicted tendencies

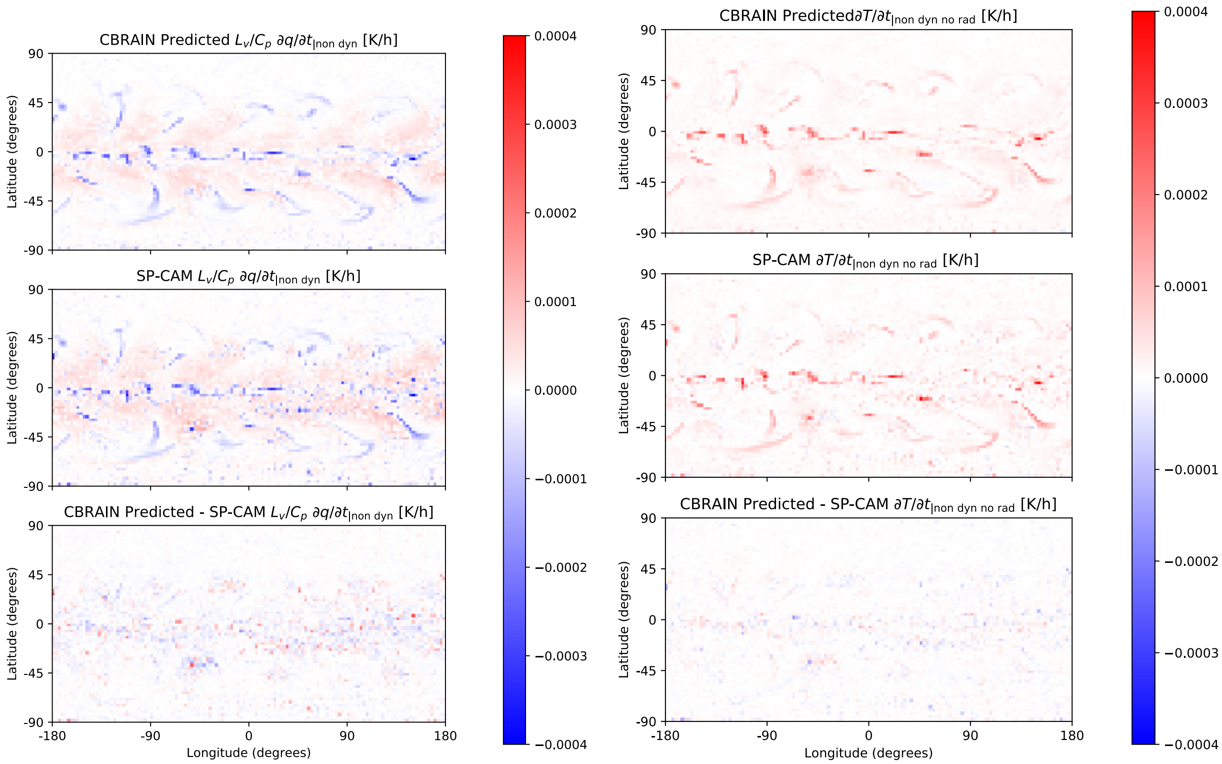

Figure 2: (left) Snapshot (Year 2, January 1, 0:00AM) of meridional and vertical comparison of convective heating rate predicted by CBRAIN (top) compared to SP-CAM (middle) and their difference (bottom); (right) same but for moistening tendencies.

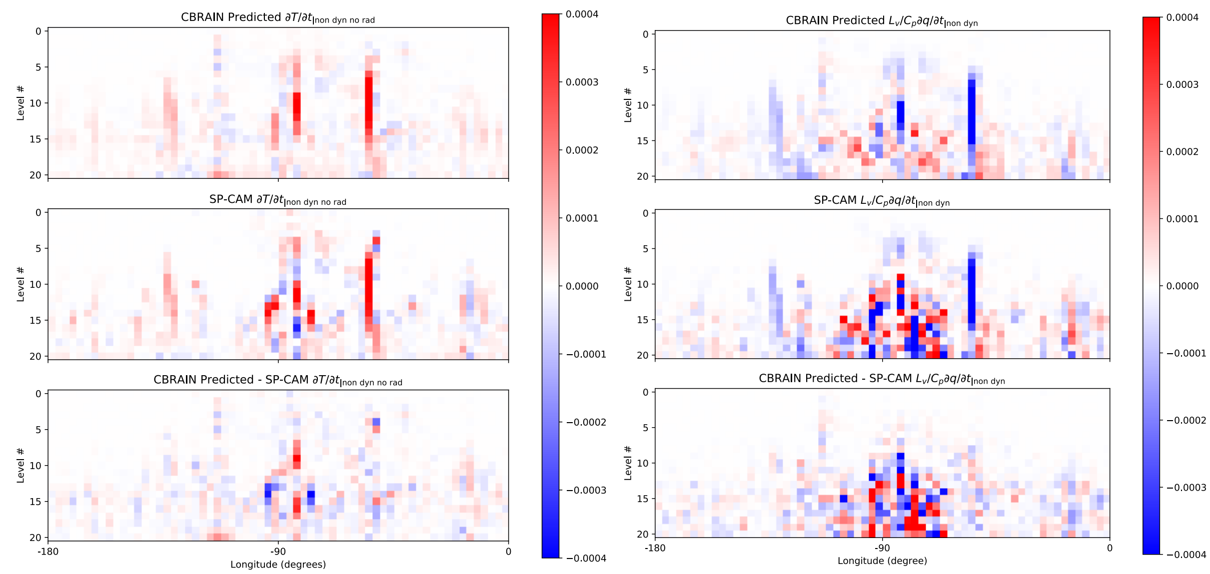

Figure 3: (left) Snapshot (Year 2, January 1, 0:00AM) of vertical and meridional comparison of convective heating rate predicted by CBRAIN (top) compared to SP-CAM (middle) and their difference (bottom); (right) same but for moistening tendencies.

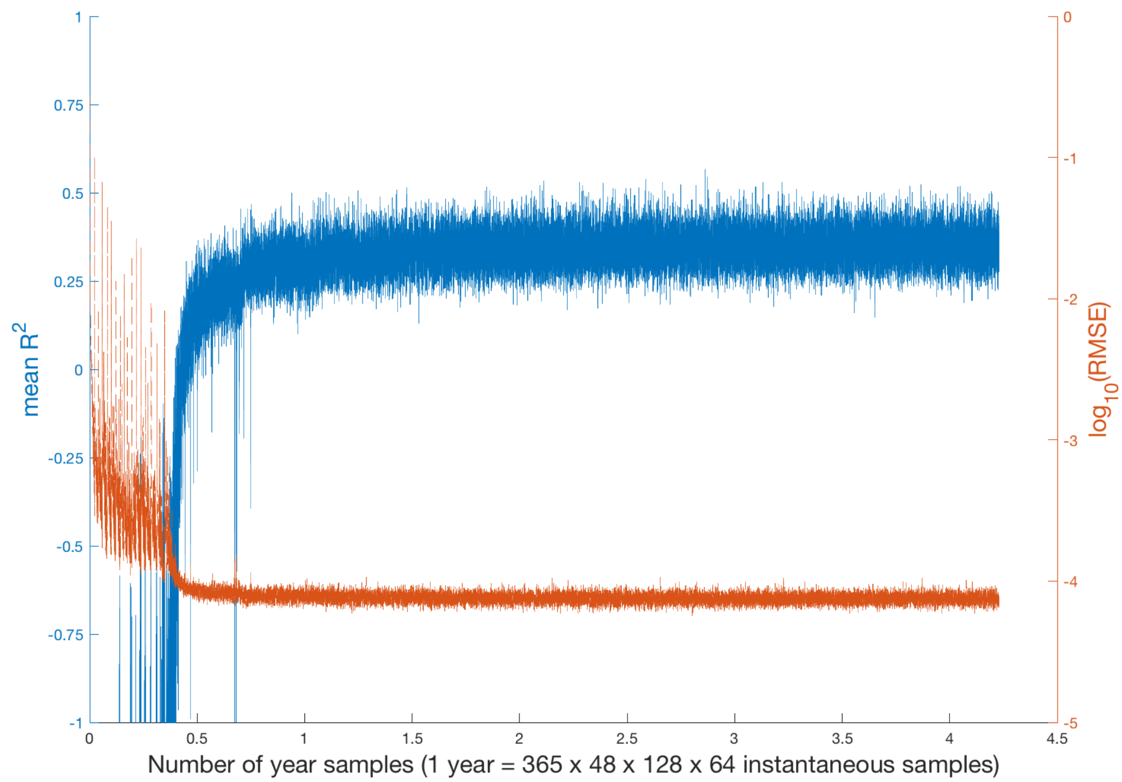

Figure S1: Impact of size of the training data

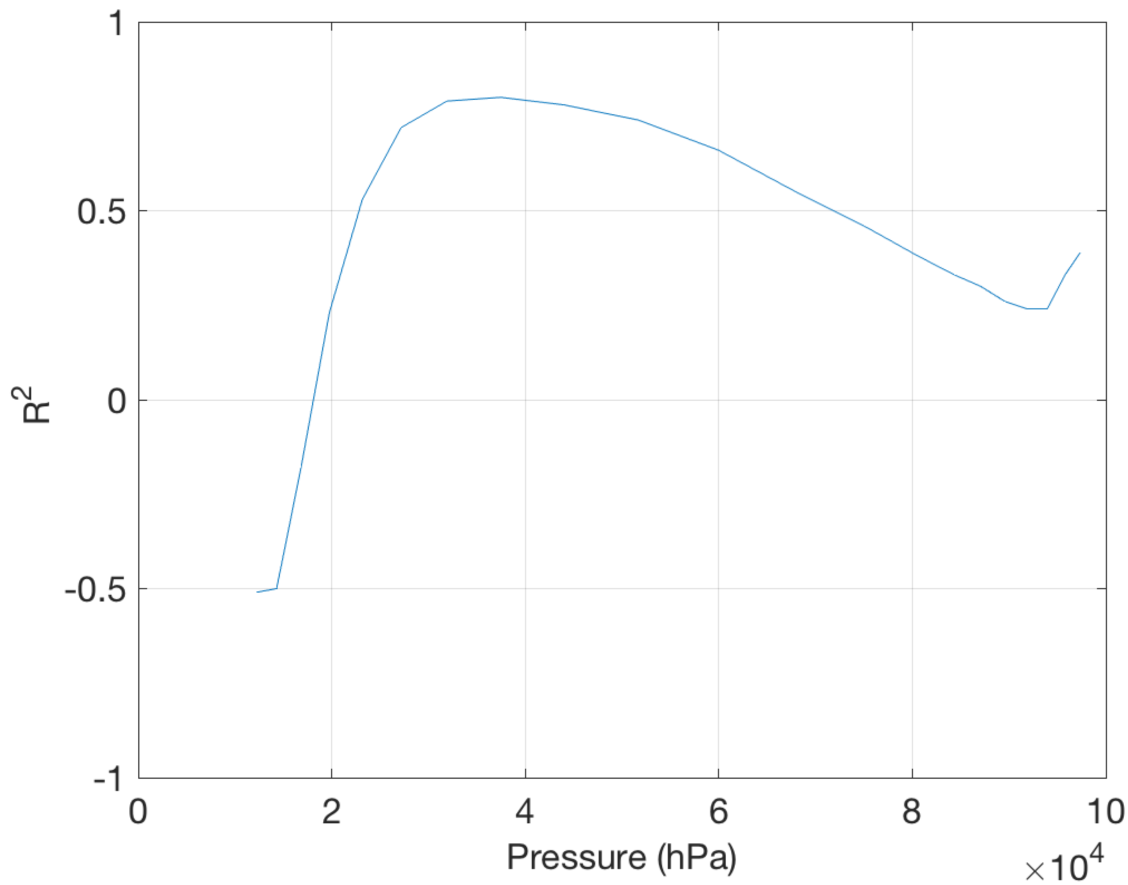

Figure S2: Final NN R^2 statistics, as a function of model level pressure

layers	RMSE	Log10(RMSE)	mse	loss	Abs(loss)	R2	mape
4096,4096	7.47E-05	-4.13	5.60E-09	5.60E-09	2.88E-05	0.36	726.04
2048,2048	7.53E-05	-4.12	5.69E-09	5.69E-09	2.87E-05	0.35	556.42
1024,1024	**7.56E-05**	**-4.12**	**5.75E-09**	**5.75E-09**	**2.89E-05**	**0.33**	**528.85**
2048,2048, 2048,2048	7.68E-05	-4.12	5.93E-09	5.93E-09	2.96E-05	0.32	685.66
256,256	7.70E-05	-4.11	5.97E-09	5.97E-09	2.98E-05	0.32	522.73
512,512	7.68E-05	-4.12	5.92E-09	5.92E-09	2.96E-05	0.32	513.54
2048,2048, 2048,2048, 2048,2048	7.76E-05	-4.11	6.06E-09	6.06E-09	3.06E-05	0.31	956.90
1024,1024, 1024,1024	7.66E-05	-4.12	5.89E-09	5.89E-09	2.97E-05	0.31	631.32

4096,4096, 4096,4096	7.81E-05	-4.11	6.12E-09	6.12E-09	3.36E-05	0.31	1797.01
512,512, 512,512	7.79E-05	-4.11	6.11E-09	6.11E-09	3.04E-05	0.30	666.19
128,128	7.88E-05	-4.11	6.24E-09	6.24E-09	3.05E-05	0.29	542.96
1024,1024,1024,1024,1024,1024	7.86E-05	-4.11	6.21E-09	6.21E-09	3.05E-05	0.29	806.71
256,256, 256,256	7.85E-05	-4.11	6.19E-09	6.19E-09	3.05E-05	0.27	675.93
512,512,512, 512,512,512	7.92E-05	-4.10	6.30E-09	6.30E-09	3.08E-05	0.27	765.12
4096,4096, 4096,4096, 4096,4096	8.01E-05	-4.10	6.44E-09	6.44E-09	3.83E-05	0.27	3436.63
100000	7.87E-05	-4.10	6.21E-09	6.21E-09	3.31E-05	0.26	1152.85
64,64	8.14E-05	-4.09	6.66E-09	6.66E-09	3.20E-05	0.25	812.46
128,128, 128,128	8.10E-05	-4.09	6.60E-09	6.60E-09	3.18E-05	0.25	742.87
256,256,256, 256,256,256	8.09E-05	-4.09	6.58E-09	6.58E-09	3.15E-05	0.24	759.46
32,32	8.22E-05	-4.09	6.80E-09	6.80E-09	3.26E-05	0.22	837.81
64,64,64,64	8.18E-05	-4.09	6.72E-09	6.72E-09	3.21E-05	0.22	809.17
32,32,32,32	8.33E-05	-4.08	6.97E-09	6.97E-09	3.31E-05	0.21	1068.68
128,128,128, 128,128,128	8.27E-05	-4.08	6.88E-09	6.88E-09	3.21E-05	0.21	752.63
64,64,64,64, 64,64	8.28E-05	-4.08	6.89E-09	6.89E-09	3.22E-05	0.20	839.99
32,32,32,32	8.21E-05	-4.09	6.76E-09	6.76E-09	3.24E-05	0.20	890.69
32,32,32,32, 32,32	8.40E-05	-4.08	7.09E-09	7.09E-09	3.29E-05	0.19	928.60
16,16	8.46E-05	-4.07	7.19E-09	7.19E-09	3.30E-05	0.19	669.42
32,32,32,32, 32,32	8.39E-05	-4.08	7.06E-09	7.06E-09	3.29E-05	0.18	950.57
16,16,16,16	8.52E-05	-4.07	7.30E-09	7.30E-09	3.40E-05	0.17	991.54
16,16,16,16, 16,16	8.50E-05	-4.07	7.27E-09	7.27E-09	3.35E-05	0.16	1028.93
10000,10000	4.40E-04	-3.45	3.78E-07	3.78E-07	3.36E-04	-41.73	76964.35
1 000 000	1.09E-01	-2.00	1.62E-01	1.62E-01	7.67E-02	-18904102.85	17001926.50

Table S 1: Statistics of the different feedforward neural networks with various congurations. ranked in descending R squared

layers	RMSE	Log10(RMSE)	mse	loss	Abs(loss)	R2	mape	layers
128,128,128,128	7.91E-05	-4.10	6.29E-09	6.29E-09	-5.05	3.15E-05	0.29	1.24E+03
512,512,512,512	7.88E-05	-4.10	6.23E-09	6.23E-09	-4.97	3.23E-05	0.29	1.78E+03
256,25,256,256	7.86E-05	-4.11	6.21E-09	6.21E-09	-5.09	3.10E-05	0.28	1.04E+03
256,25,256,2566	7.91E-05	-4.10	6.28E-09	6.28E-09	-4.99	3.23E-05	0.28	1.67E+03
512,512	8.00E-05	-4.10	6.43E-09	6.43E-09	-5.03	3.19E-05	0.28	1.46E+03
256,25,256,256,256,256	7.97E-05	-4.10	6.38E-09	6.38E-09	-5.06	3.16E-05	0.28	1.20E+03
256,256	7.91E-05	-4.10	6.28E-09	6.28E-09	-5.09	3.11E-05	0.27	1.09E+03
64,64,64,64	7.91E-05	-4.10	6.30E-09	6.30E-09	-5.09	3.13E-05	0.27	1.08E+03
128,128,128,128,128,128	7.91E-05	-4.10	6.28E-09	6.28E-09	-5.06	3.16E-05	0.27	1.19E+03
64,64,64,64,64,64	7.99E-05	-4.10	6.41E-09	6.41E-09	-5.08	3.17E-05	0.26	1.11E+03
1024,1024	8.10E-05	-4.09	6.59E-09	6.59E-09	-4.91	3.44E-05	0.26	2.38E+03
128,128	8.17E-05	-4.09	6.72E-09	6.72E-09	-5.08	3.21E-05	0.25	1.09E+03
64,64	8.13E-05	-4.09	6.65E-09	6.65E-09	-5.05	3.23E-05	0.22	1.22E+03
2048,2048	8.41E-05	-4.08	7.11E-09	7.11E-09	-4.81	3.75E-05	0.19	3.28E+03
10000	8.32E-05	-4.08	6.97E-09	6.97E-09	-4.87	3.61E-05	0.19	2.77E+03
512,512,512,512,512,512	8.69E-05	-4.06	7.58E-09	7.58E-09	-4.73	4.10E-05	0.14	4.05E+03
1024,1024,1024,1024	7.19E-04	-3.30	1.88E-06	1.88E-06	-3.68	5.08E-04	-218.36	1.25E+05
100000	7.39E-04	-3.44	2.50E-06	2.50E-06	-3.79	5.92E-04	-284.27	1.29E+05
4096,4096	1.62E-03	-2.98	7.59E-06	7.59E-06	-3.38	1.15E-03	-801.63	2.66E+05
2048,2048,2048,2048	5.13E-03	-2.53	1.30E-04	1.30E-04	-2.92	3.67E-03	-14833.57	8.39E+05
1024,1024,1024,1024,1024,1024	1.74E-02	-1.90	7.34E-04	7.34E-04	-2.32	1.16E-02	-81077.36	2.27E+06
1024,1024,1024,1024,024,1024	6.29E-03	-3.05	1.72E-03	1.72E-03	-3.37	3.54E-03	-217986.04	5.97E+05
2048,2048,2048,2048,2048,2048	3.70E-01	-0.50	2.04E-01	2.04E-01	-0.94	2.35E-01	-24015813.82	5.81E+07

Table S 2: same as Table S 1 but for the convolutional NN

References

Alemohammad, S. H., B. Fang, A. G. Konings, J. K. Green, J. Kolassa, C. Prigent, F. Aires, D. Miralles, and P. Gentine (2016), Water, Energy, and Carbon with Artificial Neural Networks (WECANN): A statistically-based estimate of global surface turbulent fluxes using solar-induced fluorescence,, 1–36, doi:10.5194/bg-2016-495.

Arnold, N. P., and D. A. Randall (2015), Global-scale convective aggregation: Implications for the Madden-Julian Oscillation, *J. Adv. Model. Earth Syst.*, *7*(4), 1499–1518, doi:10.1002/2015MS000498.

Arnold, N. P., M. Branson, M. A. Burt, D. S. Abbot, Z. Kuang, D. A. Randall, and E. Tziperman (2014), Effects of explicit atmospheric convection at high CO2, *PNAS*, *111*(30), 10943–10948, doi:10.1073/pnas.1407175111.

Benedict, J. J., and M. S. Pritchard (2015), Sensitivity of MJO propagation to a robust positive Indian Ocean dipole event in the superparameterized CAM, *Journal of Advances in Modeling Earth Systems*, doi:10.1002/2015MS000530/pdf.

Bony, S. et al. (2015), Clouds, circulation and climate sensitivity, *Nat Geosci*, *8*(4), 261–268, doi:10.1038/ngeo2398.

Bretherton, C. S., and M. F. Khairoutdinov (2015), Convective self-aggregation feedbacks in near-global cloud-resolving simulations of an aquaplanet, *J. Adv. Model. Earth Syst.*, *7*(4), 1765–1787, doi:10.1002/2015MS000499.

Bush, S. J., A. G. Turner, S. J. Woolnough, G. M. Martin, and N. P. Klingaman (2015), The effect of increased convective entrainment on Asian monsoon biases in the MetUM general circulation model, *Q J Roy Meteor Soc*, *141*(686), 311–326, doi:10.1002/qj.2371.

Cheng, A., and K.-M. Xu (2014), An Explicit Representation of Vertical Momentum Transport in a Multiscale Modeling Framework through its 2D Cloud-Resolving Model Component, *J Geophys Res-Atmos*, n/a–n/a, doi:10.1002/2013JD021078.

Chevallier, F., J. J. Morcrette, F. Cheruy, and N. A. Scott (2000), Use of a neural-network-based long-wave radiative-transfer scheme in the ECMWF atmospheric model, *Q J Roy Meteor Soc*, *126*(563), 761–776, doi:10.1002/qj.49712656318.

Cohen, C. (2000), A Quantitative Investigation of Entrainment and Detrainment in Numerically Simulated Cumulonimbus Clouds, *J Atmos Sci*, *57*(10), 1657–1674.

Coppin, D., and S. Bony (2015), Physical mechanisms controlling the initiation of convective self-aggregation in a General Circulation Model, *J. Adv. Model. Earth Syst.*, *7*(4), 2060–2078, doi:10.1002/2015MS000571.

Couvreux, F. et al. (2015), Representation of daytime moist convection over the semi-arid Tropics by parametrizations used in climate and meteorological models, *Q J Roy Meteor Soc*, *141*(691), 2220–2236, doi:10.1002/qj.2517.

Dahl, G. E., Dong Yu, Li Deng, and A. Acero (2011), Context-Dependent Pre-Trained Deep Neural Networks for Large-Vocabulary Speech Recognition, *IEEE Trans. Audio Speech Lang. Process.*, *20*(1), 30–42, doi:10.1109/TASL.2011.2134090.

Daleu, C. L. et al. (2015), Intercomparison of methods of coupling between convection and large-scale circulation: 1. Comparison over uniform surface conditions, *J. Adv. Model. Earth Syst.*, *7*(4), 1576–1601, doi:10.1002/2015MS000468.

Daleu, C. L. et al. (2016), Intercomparison of methods of coupling between convection and large-scale circulation: 2. Comparison over nonuniform surface conditions, *J. Adv. Model. Earth Syst.*, n/a–n/a, doi:10.1002/2015MS000570.

Dawe, J. T., and P. H. Austin (2013), Direct entrainment and detrainment rate distributions of individual shallow cumulus clouds in an LES, *Atmos. Chem. Phys*, *13*(15), 7795–7811, doi:10.5194/acp-13-7795-2013.

De Rooy, W. C., P. Bechtold, K. Froehlich, C. Hohenegger, H. Jonker, D. Mironov, A. P. Siebesma, J. Teixeira, and J.-I. Yano (2013), Entrainment and detrainment in cumulus convection: an overview, *Q J Roy Meteor Soc*, *139*(670), 1–19, doi:10.1002/qj.1959.

Del Genio, A. D., and J. Wu (2010), The Role of Entrainment in the Diurnal Cycle of Continental Convection, *J Climate*, *23*(10), 2722–2738, doi:10.1175/2009JCLI3340.1.

Derbyshire, S., I. Beau, P. Bechtold, J. Grandpeix, J. Piriou, J. Redelsperger, and P. M. M. Soares (2004), Sensitivity of moist convection to environmental humidity, *Q J Roy Meteor Soc*, *130*(604), 3055–3079, doi:10.1256/qj.03.130.

Dorrestijn, J., D. T. Crommelin, A. P. Siebesma, H. J. J. Jonker, and C. Jakob (2014), Stochastic parameterization of convective area fractions with a multicloud model inferred from observational data, *J Atmos Sci*, 141110132156008, doi:10.1175/JAS-D-14-0110.1.

D'Andrea, F., P. Gentine, and A. K. Betts (2014), Triggering deep convection with a probabilistic plume model, *J Atmos Sci*, *71*(11), 3881–3901, doi:10.1175/JAS-D-13-0340.1.

Feng, Z., S. Hagos, A. K. Rowe, C. D. Burleyson, M. N. Martini, and S. P. de Szoeke (2015), Mechanisms of convective cloud organization by cold pools over tropical warm ocean during the AMIE/DYNAMO field campaign, *J. Adv. Model. Earth Syst.*, *7*(2), 357–381, doi:10.1002/2014MS000384.

Gentine, P., A. Garelli, S. B. Park, and J. Nie (2016), Role of surface heat fluxes underneath cold pools, *Geo Res Letters*, *43*(2), 874–883, doi:10.1002/2015GL067262.

Goswami, B. B., P. Mukhopadhyay, M. Khairoutdinov, and B. N. Goswami (2013), Simulation of Indian summer monsoon intraseasonal oscillations in a superparameterized coupled climate model: need to improve the embedded cloud resolving model, *Climate dynamics*, *41*(5-6), 1497–1507, doi:10.1007/s00382-012-1563-1.

Guichard, F. et al. (2004), Modelling the diurnal cycle of deep precipitating convection over land with cloud-resolving models and single-column models, *Q J Roy Meteor Soc*, *130*(604), 3139–3172, doi:10.1256/qj.03.145.

Hinton, G. et al. (2012), Deep Neural Networks for Acoustic Modeling in Speech Recognition: The Shared Views of Four Research Groups, *IEEE Signal Process. Mag.*, *29*(6), 82–97, doi:10.1109/MSP.2012.2205597.

Hohenegger, C., and B. Stevens (2016), Coupled radiative convective equilibrium simulations with explicit and parameterized convection, *J. Adv. Model. Earth Syst.*, *8*(3), 1468–1482, doi:10.1002/2016MS000666.

Hohenegger, C., L. Schlemmer, and L. Silvers (2015), Coupling of convection and circulation at various resolutions, *Tellus Series A-Dynamic Meteorology And Oceanography*, *67*(0), doi:10.3402/tellusa.v67.26678.

Hohenegger, C., P. Brockhaus, C. S. Bretherton, and C. Schaer (2009), The Soil Moisture-Precipitation Feedback in Simulations with Explicit and Parameterized Convection, *J Climate*, *22*(19), 5003–5020, doi:10.1175/2009JCLI2604.1.

Holloway, C. E. (2017), Convective aggregation in realistic convective-scale simulations, *J. Adv. Model. Earth Syst.*, *7*(608), 1499–68, doi:10.1002/2017MS000980.

Houze, R. A. (2004), Mesoscale convective systems, *Reviews of Geophysics*, *42*(4), RG4003, doi:10.1029/2004RG000150.

Jeevanjee, N., and D. M. Romps (2013), Convective self-aggregation, cold pools, and domain size, *Geophys Res Lett*, *40*(5), 994–998, doi:10.1002/grl.50204.

Jimenez, C., C. Prigent, and F. Aires (2009), Toward an estimation of global land surface heat fluxes from multisatellite observations, *J Geophys Res-Atmos*, *114*(D6), D06305–, doi:10.1029/2008JD011392.

Karabatak, M., and M. C. Ince (2009), An expert system for detection of breast cancer based on association rules and neural network, *Expert Systems With Applications*, *36*(P2), 3465–3469, doi:10.1016/j.eswa.2008.02.064.

Khairoutdinov, M. F., S. K. Krueger, C.-H. Moeng, P. A. Bogenschutz, and D. A. Randall (2009), Large-eddy simulation of maritime deep tropical convection, *J. Adv. Model. Earth Syst.*, *2*, 15, doi:10.3894/JAMES.2009.1.15.S1.

Khairoutdinov, M., and D. Randall (2006), High-resolution simulation of shallow-to-deep convection transition over land, *J Atmos Sci*, *63*(12), 3421–3436.

Khairoutdinov, M., D. Randall, and C. DeMott (2005), Simulations of the Atmospheric General Circulation Using a Cloud-Resolving Model as a Superparameterization of Physical Processes, *Journal of Atmospheric Sciences*, *62*(7), 2136–2154, doi:10.1175/JAS3453.1.

Khan, J., J. S. Wei, M. Ringner, L. H. Saal, and M. Ladanyi (2001), Classification and diagnostic prediction of cancers using gene expression profiling and artificial neural networks, *Nature*.

Khouider, B., A. Majda, and M. Katsoulakis (2003), Coarse-grained stochastic models for tropical convection and climate, *P Natl Acad Sci Usa*, *100*(21), 11941–11946, doi:10.1073/pnas.1634951100.

Khouider, B., and A. Majda (2006), A simple multicloud parameterization for convectively coupled tropical waves. Part I: Linear analysis, *J Atmos Sci*, *63*(4), 1308–1323.

Khouider, B., J. Biello, and A. J. Majda (2010), A stochastic multicloud model for tropical convection, *Commun Math Sci*, *8*(1), 187–216.

Kim, D., A. H. Sobel, A. D. Del Genio, Y. Chen, S. J. Camargo, M.-S. Yao, M. Kelley, and L. Nazarenko (2012), The Tropical Subseasonal Variability Simulated in the NASA GISS General Circulation Model, *J Climate*, *25*(13), 4641–4659, doi:10.1175/JCLI-D-11-00447.1.

Kolassa, J., F. Aires, J. Polcher, C. Prigent, C. Jimenez, and J. M. Pereira (2013), Soil moisture retrieval from multi-instrument observations: Information content analysis and retrieval methodology, *J Geophys Res-Atmos*, *118*(10), 4847–4859, doi:10.1029/2012JD018150.

Kolassa, J., P. Gentine, C. Prigent, and F. Aires (2016), Soil moisture retrieval from AMSR-E and ASCAT microwave observation synergy. Part 1: Satellite data analysis, *Remote Sensing of Environment*, *173*, 1–14, doi:10.1016/j.rse.2015.11.011.

Kolassa, J., P. Gentine, C. Prigent, F. Aires, and S. H. Alemohammad (2017a), Soil moisture retrieval from AMSR-E and ASCAT microwave observation synergy. Part 2: Product evaluation, *Remote Sensing of Environment*, *195*, 202–217, doi:10.1016/j.rse.2017.04.020.

Kolassa, J., R. H. Reichle, and C. S. Draper (2017b), Merging active and passive microwave observations in soil moisture data€assimilation, *Remote Sensing of Environment*, *191*(C), 117–130, doi:10.1016/j.rse.2017.01.015.

Kooperman, G. J., M. S. Pritchard, and R. C. J. Somerville (2013), Robustness and sensitivities of central US summer convection in the super-parameterized CAM: Multi-model intercomparison with a new regional EOF index, *Geophys Res Lett*, *40*(12), 3287–3291, doi:10.1002/grl.50597.

Kooperman, G. J., M. S. Pritchard, and R. C. J. Somerville (2014), The response of US summer rainfall to quadrupled CO 2climate change in conventional and superparameterized versions of the NCAR Community Atmosphere Model, *J. Adv. Model. Earth Syst.*, n/a–n/a, doi:10.1002/2014MS000306.

Kooperman, G. J., M. S. Pritchard, M. A. Burt, M. D. Branson, and D. A. Randall (2016a), Impacts of cloud superparameterization on projected daily rainfall intensity climate changes in multiple versions of the Community Earth System Model, *J. Adv. Model. Earth Syst.*, 1–73, doi:10.1002/2016MS000715.

Kooperman, G. J., M. S. Pritchard, M. A. Burt, M. D. Branson, and D. A. Randall (2016b), Robust effects of cloud superparameterization on simulated daily rainfall intensity statistics across multiple versions of the Community Earth System Model, *J. Adv. Model. Earth Syst.*, n/a–n/a, doi:10.1002/2015MS000574.

Krizhevsky, A., I. Sutskever, and G. E. Hinton (2017), ImageNet classification with deep convolutional neural networks, *Commun. ACM*, *60*(6), 84–90, doi:10.1145/3065386.

LeCun, Y., Y. Bengio, and G. Hinton (2015), Deep learning, *Nature*, *521*(7553), 436–444, doi:10.1038/nature14539.

Lu, C., Y. Liu, G. J. Zhang, X. Wu, S. Endo, L. Cao, Y. Li, and X. Guo (2016), Improving Parameterization of Entrainment Rate for Shallow Convection with Aircraft Measurements and Large-Eddy Simulation, *Journal of Atmospheric Sciences*, *73*(2), 761–773, doi:10.1175/JAS-D-15-0050.1.

Mapes, B., and R. Neale (2011), Parameterizing Convective Organization to Escape the Entrainment Dilemma, *J. Adv. Model. Earth Syst.*, *3*(6), M06004, doi:10.1029/2011MS000042.

Medeiros, B., B. Stevens, and S. Bony (2014), Using aquaplanets to understand the robust responses of comprehensive climate models to forcing, *Climate dynamics*, *44*(7-8), 1957–1977, doi:10.1007/s00382-014-2138-0.

Miao, C., H. Ashouri, K.-L. Hsu, S. Sorooshian, and Q. Duan (2015), Evaluation of the PERSIANN-CDR Daily Rainfall Estimates in Capturing the Behavior of Extreme Precipitation Events over China, *J Hydrometeorol*, *16*(3), 1387–1396, doi:10.1175/JHM-D-14-0174.1.

Moazami, S., S. Golian, M. R. Kavianpour, and Y. Hong (2013), Comparison of PERSIANN and V7 TRMM Multi- satellite Precipitation Analysis (TMPA) products with rain gauge data over Iran, *International Journal of Remote Sensing*, *34*(22), 8156–8171, doi:10.1080/01431161.2013.833360.

Moncrieff, M. W., and C. Liu (2006), Representing convective organization in prediction models by a hybrid strategy, *J Atmos Sci*, *63*(12), 3404–3420.

Muller, C., and S. Bony (2015), What favors convective aggregation and why? *Geophys Res Lett*, *42*(13), 5626–5634, doi:10.1002/2015GL064260.

Nie, J., and A. H. Sobel (2016), Modeling the Interaction between Quasigeostrophic Vertical Motion and Convection in a Single Column, *Journal of Atmospheric Sciences*, *73*(3), 1101–1117, doi:10.1175/JAS-D-15-0205.1.

Nie, J., D. A. Shaevitz, and A. H. Sobel (2016), Forcings and feedbacks on convection in the 2010 Pakistan flood: Modeling extreme precipitation with interactive large-scale ascent, *J. Adv. Model. Earth Syst.*, 1–47, doi:10.1002/2016MS000663.

Oueslati, B., and G. Bellon (2015), The double ITCZ bias in CMIP5 models: interaction between SST, large-scale circulation and precipitation, *Climate dynamics*, doi:10.1007/s00382-015-2468-6.

Pauluis, O., and J. Schumacher (2011), Self-aggregation of clouds in conditionally unstable moist convection, *P Natl Acad Sci Usa*, *108*(31), 12623–12628, doi:10.2307/27979061?ref=no-x-route:c1a463f61022111b992ca603578ce8ea.

Popke, D., B. Stevens, and A. Voigt (2013), Climate and climate change in a radiative-convective equilibrium version of ECHAM6, *J. Adv. Model. Earth Syst.*, *5*(1), 1–14, doi:10.1029/2012MS000191.

Pritchard, M. S., and R. C. J. Somerville (2009), Assessing the Diurnal Cycle of Precipitation in a Multi-Scale Climate Model, *J. Adv. Model. Earth Syst.*, *1*, doi:10.3894/JAMES.2009.1.12.

Pritchard, M. S., C. S. Bretherton, and C. A. Demott (2014), Restricting 32–128 km horizontal scales hardly affects the MJO in the Superparameterized Community Atmosphere Model v.3.0 but the number of cloud-resolving grid columns constrains vertical mixing, *J. Adv. Model. Earth Syst.*, *6*(3), 723–739, doi:10.1002/2014MS000340.

Pritchard, M. S., M. W. Moncrieff, and R. C. J. Somerville (2011), Orogenic Propagating Precipitation Systems over the United States in a Global Climate Model with Embedded Explicit Convection, *Journal of Atmospheric Sciences*, *68*(8), 1821–1840, doi:10.1175/2011JAS3699.1.

Rochetin, N., F. Couvreux, J.-Y. Grandpeix, and C. Rio (2014a), Deep Convection Triggering by Boundary Layer Thermals. Part I: LES Analysis and Stochastic Triggering Formulation, *J Atmos Sci*, *71*(2), 496–514, doi:10.1175/JAS-D-12-0336.1.

Rochetin, N., J.-Y. Grandpeix, C. Rio, and F. Couvreux (2014b), Deep Convection Triggering by Boundary Layer Thermals. Part II: Stochastic Triggering Parameterization for the LMDZ GCM, *J Atmos Sci*, *71*(2), 515–538, doi:10.1175/JAS-D-12-0337.1.

Romps, D. M. (2010), A Direct Measure of Entrainment, *J Atmos Sci*, *67*(6), 1908–1927, doi:10.1175/2010JAS3371.1.

Seiki, T., C. Kodama, A. T. Noda, and M. Satoh (2015), Improvement in Global Cloud-System-Resolving Simulations by Using a Double-Moment Bulk Cloud Microphysics Scheme, *J Climate*, *28*(6), 2405–2419, doi:10.1175/JCLI-D-14-00241.1.

Sherwood, S. C., and D. Hernández-Deckers (2013), Slippery thermals and the cumulus entrainment paradox*, *J Atmo Sci*, *70*(8), 2426–2442.

Sherwood, S. C., S. Bony, and J. L. Dufresne (2014), Spread in model climate sensitivity traced to atmospheric convective mixing, *Nature*, *505*(7481), 37–42, doi:10.1038/nature12829.

Silver, D. et al. (2016), Mastering the game of Go with deep neural networks and tree search, *Nature*, *529*(7585), 484–489, doi:10.1038/nature16961.

Singh, M. S., and P. A. O'Gorman (2013), Influence of entrainment on the thermal stratification in simulations of radiative-convective equilibrium, *Geophys Res Lett*, *40*(16), 4398–4403, doi:10.1002/grl.50796.

Stevens, B., and S. Bony (2013), What Are Climate Models Missing? *Science*, *340*(6136), 1053–1054, doi:10.1126/science.1237554.

Sun, J., and M. S. Pritchard (2016), Effects of explicit convection on global land-atmosphere coupling in the superparameterized CAM, *J. Adv. Model. Earth Syst.*, 1–22, doi:10.1002/2016MS000689.

Tan, J., C. Jakob, W. B. Rossow, and G. Tselioudis (2015), Increases in tropical rainfall driven by changes in frequency of organized deep convection, *Nature*, *519*(7544), 451–+, doi:10.1038/nature14339.

Tao, Y., X. Gao, K. Hsu, S. Sorooshian, and A. Ihler (2016), A Deep Neural Network Modeling Framework to Reduce Bias in Satellite Precipitation Products, *J Hydrometeorol*, *17*(3), 931–945, doi:10.1175/JHM-D-15-0075.1.

Taylor, C. M., C. E. Birch, D. J. Parker, N. Dixon, F. Guichard, G. Nikulin, and G. M. S. Lister (2013), Modelling soil moisture - precipitation feedbacks in the Sahel: importance of spatial scale versus convective parameterization, *Geophys Res Lett*, *40*(23), 6213–6218, doi:10.1002/2013GL058511.

Taylor, C. M., P. P. Harris, and D. J. Parker (2009), Impact of soil moisture on the development of a Sahelian mesoscale convective system: a case-study from the AMMA Special Observing Period, *Q J Roy Meteor Soc*, *136*(S1), 456–470, doi:10.1002/qj.465.

Tian, Y., and Z. Kuang (2016), Dependence of entrainment in shallow cumulus convection on vertical velocity and distance to cloud edge, *Geophys Res Lett*, *43*(8), 4056–4065, doi:10.1002/2016GL069005.

Tobin, I., S. Bony, C. E. Holloway, J.-Y. Grandpeix, G. Sèze, D. Coppin, S. J. Woolnough, and R. Roca (2013), Does convective aggregation need to be represented in cumulus parameterizations? *J. Adv. Model. Earth Syst.*, n/a–n/a, doi:10.1002/jame.20047.

Wing, A. A., and K. A. Emanuel (2014), Physical mechanisms controlling self-aggregation of convection in idealized numerical modeling simulations, *J. Adv. Model. Earth Syst.*, *6*(1), 59–74, doi:10.1002/2013MS000269.

Wing, A. A., K. Emanuel, C. E. Holloway, and C. Muller (2017), Convective Self-Aggregation in Numerical Simulations: A Review, *Surv Geophys*, *38*(6), 1173–1197, doi:10.1007/s10712-017-9408-4.

Wu, C.-M., B. Stevens, and A. Arakawa (2009), What Controls the Transition from Shallow to Deep Convection? *J Atmos Sci*, *66*(6), 1793–1806, doi:10.1175/2008JAS2945.1.

Yeo, K., and D. M. Romps (2013), Measurement of Convective Entrainment Using Lagrangian Particles, *J Atmos Sci*, *70*(1), 266–277, doi:10.1175/JAS-D-12-0144.1.

Yu, S., and M. S. Pritchard (2015), The effect of large-scale model time step and multiscale coupling frequency on cloud climatology, vertical structure, and rainfall extremes in a superparameterized GCM, *J. Adv. Model. Earth Syst.*, *7*(4), 1977–1996, doi:10.1002/2015MS000493.

Zhou, Z. H., Y. Jiang, Y. B. Yang, and S. F. Chen (2002), Lung cancer cell identification based on artificial neural network ensembles, *Artificial Intelligence in Medicine*, *24*(1), 25–36.